Angle-resolved energy dependence of the $4p^4nd(^2S_{1/2})$ $(n=4-7)$ correlation satellites in Kr from 38.5 to 250 eV: Experiment and theory

N. Berrah,[1] A. Farhat,[1] B. Langer,[1,2] B. M. Lagutin,[3] Ph. V. Demekhin,[3] I. D. Petrov,[3] V. L. Sukhorukov,[3] R. Wehlitz,[4] S. B. Whitfield,[5] J. Viefhaus,[2] and U. Becker[2]

[1]*Physics Department, Western Michigan University, Kalamazoo, Michigan 49008*

[2]*Fritz-Haber-Institut der Max-Planck-Gesellschaft, Faradayweg 4-6, D-14195, Berlin, Germany*

[3]*Rostov State University, Rostov-on-Don 344017, Russia*

[4]*Physics Department, University of Tennessee, Knoxville, Tennessee 37996-1200*

[5]*Physics Department, University of South Alabama, Mobile, Alabama 36688-0002*

(Received 16 June 1997)

We measured and calculated the energy dependence of the $4p^4nd(^2S_{1/2})$ $(n=4-7)$ correlation satellites in Kr from 38.5 to 250 eV. Our high-resolution measurements used a photoelectron spectroscopy technique to determine the relative cross sections and angular distribution parameters β. We find that, as in the case of Xe, the absolute cross sections of these satellites lines follow very closely the shifted and scaled cross section of the $4s$ main line. However, in the case of β, we find that the $nd(^2S_{1/2})$ $(n=4,5,6)$ follow the β value of the $4s$ main line below 150 eV only, and that β of the $7d(^2S_{1/2})$ satellite does not. We find that the β of the $nd(^2S_{1/2})$ ($n=4$, 5, and 6) satellites reach $\beta=2$ below 150 eV, but this value drops significantly between photon energies of 200 and 250 eV. While the comparison of our measurements with our calculation is good overall, some effects are not reproduced by the calculation. Our results are compared with a previous measurement at 68.5 eV, and the agreement is fair. We also measured the $4s$ and $4p$ main line cross sections and angular distributions and these results are compared to previous measurements and calculations. [S1050-2947(97)02512-2]

PACS number(s): 32.30.−r, 32.80.Fb

I. INTRODUCTION

Subvalence shells in atoms and molecules display, in their photoelectron spectra, a rich satellite structure which corresponds to excited states of the ion. Satellite lines, which are entirely due to electron correlation, and which under some circumstances can dominate the spectrum, have received a great deal of interest both experimentally [1–8] and theoretically [9–13].

The knowledge of cross sections for the population of satellite states and their angular distributions may be a key to the understanding of the electron-electron interactions in many electron systems as well as relativistic effects. A study of the angular distribution parameter β of the main ns line of the heavier rare gases is of interest because the spin-orbit interaction leads to the nonconservation of the orbital momenta of the photoelectron [14–17] and the ion core [18]. As a consequence, anomalous dependence of the behavior of β as a function of photon energy was observed [19–21]. Most experimental investigations concentrated on Ar, for which measurements [7,22–25] and calculations [26–28] are in very good agreement. In the case of Xe, a recent high-resolution experiment was performed [29], as well as calculations [18]. However, in the case of Kr, there is a definite lack of experimental data. High-energy, low-resolution data at 1.2 and 1.5 keV for the $4d$ satellite line intensity [30], and high-resolution data [3] at 1.5 keV are available. In the low-photon-energy range, only one angular-resolved measurement was done at 68.5 eV [7].

In this paper, we report a systematic study, not done previously, of the energy dependence of the Kr $4p^4nd(^2S_{1/2})$ $(n=4-7)$ correlation satellites from 38.5 to 250 eV, both experimentally, using a photoelectron spectrometry technique, and theoretically using a configuration interaction (CI) method and many-body perturbation theory. Specifically, we determined the relative cross sections $[\sigma_{ns}(h\nu)]$ and angular distribution parameters $[\beta_{ns}(h\nu)]$ for the satellites with total angular momentum $J=\frac{1}{2}$, and compared the experimental and theoretical results. This comparison shows the importance of including in the calculations initial-state configuration interaction (ISCI), final ionic-state configuration interaction (FISCI), intershell correlations in the case of the $\sigma_{ns}(h\nu)$, and the particular importance of including relativistic effects in the case of $\beta_{ns}(h\nu)$. In addition, we measured and analyzed the $4s$ and $4p$ main line cross sections and angular distributions over an extended energy range. These results, used to calibrate our data, are also compared with previous measurements and calculations.

II. EXPERIMENTAL METHOD

The experiment was performed at the Hamburger Synchrotronstrahlungslabor (HASYLAB) synchrotron radiation source on the undulator beam line (BW3) coupled with a high resolution SX-700 monochromator [31]. The measurements were carried out during timing operation of the electron storage ring using monochromatic light between 38.5 and 250 eV. Spectra were recorded using two time-of-flight spectrometers with an average nominal resolving power of 100 meV, which was enhanced by application of a retarding potential. Both analyzers were mounted on a rotatable chamber, perpendicular to the axis of the synchrotron radiation beam, enabling a determination of the electron angular distributions. One analyzer was mounted at $\theta=0°$ with respect to the electric-field axis of the photon beam and the other at

$\theta = 54.7°$, the so called ''magic angle'' (at this angle the relative intensities of the photolines are independent of angular distributions). Details of the experimental apparatus can be found in previous work [32].

In the dipole approximation for linear polarization of the incident photons, the emission of electrons is given by [21]

$$\frac{d\sigma_{if}}{d\Omega} = \frac{\sigma_{if}}{4\pi}\left[1 + \frac{\beta_{if}}{4}(1 + 3P_1\cos 2\theta)\right], \tag{1}$$

where σ_{if} is the total photoionization cross section for producing the final state $|f\rangle$ of the ion, θ is the angle between the photon's polarization vector and the photoelectron's momentum direction, β_{if} is the electron angular-distribution parameter where $-1 \leqslant \beta \leqslant 2$, and P_1 is the degree of linear polarization of the photon beam.

The spectra were excited by photons with an energy below 70 eV filtered through an aluminum foil to absorb second-order radiation which could produce Auger lines in the kinetic-energy range of interest. After subtraction of a suitable background level, the electron yield was converted from a time scale to an energy scale. This was achieved using measured spectra of Ne $2s$ and $2p$ photolines and their known binding energies [33,34] to calibrate the relevant kinetic-energy range. From these Ne calibration spectra, we also obtained the relative detection efficiency of the two analyzers. Therefore, all spectra have been corrected for the analyzer's transmission and detector efficiencies. Thus the areas under the peaks are directly proportional to the intensities of the respective process. The intensity of the lines were determined by a least χ^2 fitting procedure using Gaussian curves. The assignments of these lines were taken from Ref. [35], and the corresponding binding energies were taken from Ref. [7]. During the fitting procedure for each satellite line, we fixed the corresponding binding energy. We determined our systematic uncertainty, which takes into account the sensitivity of the fit, by performing a number of fits allowing for deviation of the peak widths. An error of 5% in the area was found in the low-photon-energy range, while 10–20 % was found between 200 and 250 eV. To determine the β parameter for each nd Rydberg satellite, we fitted the ratio of each nd satellite with respect to the $4s$ and $4p$ main lines, fixing the β parameter for the $4s$ and $4p$ main line (the values used are described in Sec. IV). The systematic uncertainties were determined to vary between 10% in the best cases and 50% in the case of the $6d$ satellites at 55 eV (they are listed in Table II).

III. THEORETICAL CALCULATION

The technique applied in the present work for the calculation of the wave functions of the initial and final atomic states and to the transition amplitudes is very similar to the technique used in our previous work [13,18,36,37], where other details can be found.

To calculate the transition amplitudes the following scheme was applied:

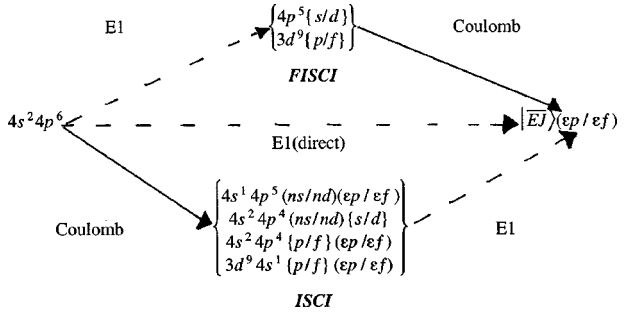

(2)

Here $|\overline{EJ}\rangle$ denotes the Kr II residual ionic state (see below), the top and bottom pathways represent correlational corrections to the amplitude of the direct $4s^2 4p^6 \rightarrow |\overline{EJ}\rangle \varepsilon p$ transition because of (FISCI) and (ISCI), respectively; $\{l\}$ indicates a complete set of intermediate atomic orbitals (AO's), over which summation and integration are carried out, broken and solid lines designate electric dipole photon excitation and Coulomb interaction, respectively. The notation (**a**/**b**) means that either the single-electron state **a** or the state **b** has been chosen in the calculation. The description of the AO's and wave functions $|\overline{EJ}\rangle$ involved in the calculation is listed below.

A. Atomic orbitals

To calculate the AO's, two approximations were used in the present paper. The first approximation is the same as in Ref. [18]. According to that work, the core AO's were calculated in the Hartree-Fock (HF) approximation. To take into account the relativistic effects in the calculation of the wave functions $|\overline{EJ}\rangle$, perturbation theory and an intermediate coupling scheme were used. To take into account the dependence of the εl AO's on the total momentum j of the photoelectron (which is necessary for the understanding of the anomalous dependence of the β parameter on photon energy [14–16]), the spin-orbit potential was included in the HF equation for the εl AO's. In the present work this approximation is called the configuration-interaction Hartree-Fock (CIHF) approximation.

The second approximation is based on the Pauli-Fock (PF) approximation applied to the calculation in Refs. [37, 38]. With regard to this approximation, mass-velocity and Darwin corrections are included in the HF equations during the self-consistent procedure for the core AO's calculation. This approximation allows one to describe the relativistic compression of the atomic core (the influence of this effect on the calculation of σ and β will be discussed below). The equation for the εl AO contains in this approximation the mass-velocity, Darwin, and the spin-orbit terms. This approximation is the so-called configuration interaction Pauli-Fock (CIPF) approximation. In all of our calculations, we only present velocity-gauge results for the cross sections and β parameters, but it should be mentioned that the difference between the length and the velocity results is very small.

In order to calculate the AO's of virtual channels $\{1\}$ and final-state photoelectrons which are contained in scheme (2), we used the frozen-core approximation [13,18,36]. Due to this approximation, the core AO's involved in scheme (2) are

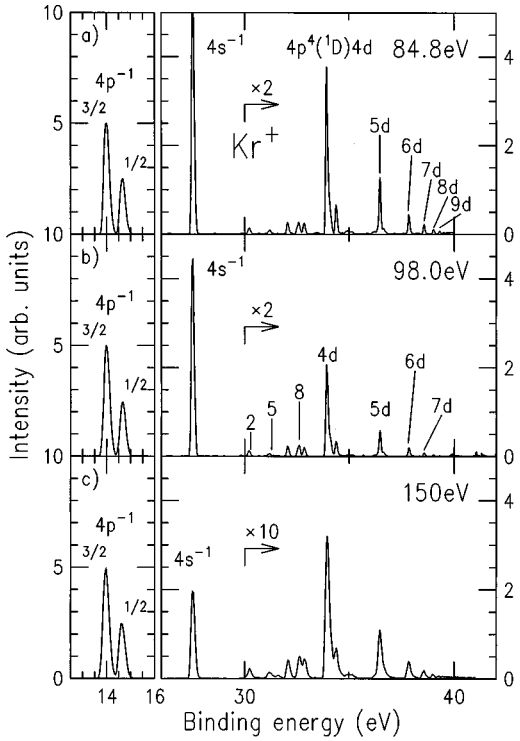

FIG. 1. High-resolution photoelectron spectra of the krypton correlation satellites recorded at three different photon energies (a) 84.8 eV, (b) 98.0 eV, and (c) 150.0 eV and at an angle of 0° with respect to the electric-field vector. The spectra are normalized to the intensity of the $4p_{3/2}^{-1}$ main line.

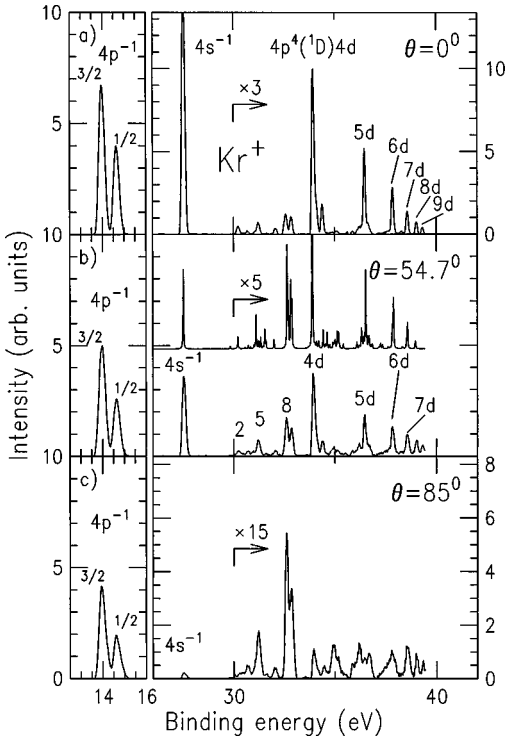

FIG. 2. High-resolution photoelectron spectra of the krypton correlation satellites recorded at a photon energy of 68.5 eV under angles of (a) 0°, (b) 54.7°, and (c) 85° with respect to the electric-field vector. The upper spectrum in the middle panel (b) is the calculated spectrum which is convoluted with a Lorentzian profile of arbitrary FWHM=30 meV to simulate the nature width of the lines. The experimental spectra are normalized to the intensity of the $4p_{3/2}^{-1}$ main line.

from the ground $4s^2 4p^6$ configuration. The AO's for the interchannel FISCI calculation were obtained in the respective nl^{-1} core and using a term dependence (term ^1P) equation. Those AO's which determine the interaction of the $4s^{-1}$ and the $4p^{-2}$ (ns/nd) configurations (dipole polarization of electron shells, DPES [13]) in the final ionic states were calculated using a $4p^{-2}$ core and an averaged $4p$-nl Coulomb interaction. It should be pointed out here that this procedure leads to the appearance of overlap integrals in the matrix elements describing FISCI. To avoid the divergence problems appearing in the ISCI calculation, the correlation function technique [13] was used.

B. Wave functions

In the present paper we applied the configuration interaction technique in order to calculate the wave functions $|\overline{EJ}\rangle$ of the final ionic state. Therefore, the CIHF or CIPF abbreviations are used regarding the AO's involved in the calculation. The wave function $|\overline{EJ}\rangle$ of the Kr II final-ionic state with definite energy E and total momentum J is a superposition of single-configurational basis states $|K\alpha\overline{LSJ}\rangle$ having definite orbital L and spin S momenta:

$$|\overline{EJ}\rangle = \sum_{K\alpha\overline{LS}} \langle K\alpha\overline{LSJ}|\overline{EJ}\rangle |K\alpha\overline{LSJ}\rangle. \tag{3}$$

In Eq. (3), K is the electron configuration of an ion, α denotes the remaining quantum numbers of the basis state (e.g., intermediate orbital and spin momenta). The expansion coefficients $\langle K\alpha\overline{LSJ}|\overline{EJ}\rangle$ are obtained by solving the respective secular equation [18]. The coefficients of the correlational decrease of the Coulomb interaction and correlation energies of each configuration K were calculated via perturbation theory described in former papers [13,18,36,37]. The decrease coefficients are 1.20, 1.38, and 1.25 for the $4p$-nl, $4p4p$-$4snl$, and interchannel Coulomb interactions, respectively. The small difference in the decrease coefficient of the interchannel interaction shown in Ref. [13] (coefficient 1.26), is connected to the use of the larger basis set of AO's in the present paper. The use of these sets also caused a small change of the correlation energies of the excited configurations K and, as a result, small differences of the energies E and wave functions $|\overline{EJ}\rangle$ from the respective quantities calculated in Ref. [13]. After the solution of the secular equations of 40, 57, 54, 30, and 12 orders for $J=\frac{1}{2}, \frac{3}{2}, \frac{5}{2}, \frac{7}{2}$, and $\frac{9}{2}$, respectively, the accuracy of the calculation of the ionic energies E is 0.05 eV. We estimate this accuracy as a standard deviation σ for the 71 calculated and measured [39] energies of the levels having the values in the 27.51–36.17-eV region. For the more excited states, the absolute accuracy of the energy calculation seems to be worse. In Table I our calculated energies are compared with the energies measured in Ref. [7]. The absolute accuracy of the energy calculation for the highly excited states could be estimated as 0.2 eV, but we expect that the relative position of highly excited levels is not worse than 0.05 eV.

The formula for the calculation of the cross section $\sigma\langle\overline{EJ}\rangle$ and angular distribution parameter $\beta\langle\overline{EJ}\rangle$ used in the present paper are the same as in the previous work [18], and will not be listed here. This technique was applied to the calculation of the cross sections of the main lines and satellite lines. For the most intense satellites characterized by $J=\frac{1}{2}$, the angular distribution parameter β was also calculated.

IV. RESULTS AND DISCUSSION

Figure 1 illustrates the highest resolution photoelectron spectra, to our knowledge, taken of the Kr valence satellites, although the 0° measurement of Ref. [17] at 68.5 eV is comparable for the lowest satellites. They were measured at three different photon energies and at $\theta=0°$ with respect to the electric-field vector. The $4s^{-1}$ and $4p^{-1}_{1/2,3/2}$ Kr^+ main lines are shown along with the rather strong $4p^4(^1D)nd(n=4-9)$ satellites at 84.8 eV. However, the satellite strength decreases as a function of increasing photon energies, as shown at 98 and 150 eV. Figure 2 shows photoelectron spectra taken at 68.5 eV for three different angles, at $\theta=0°$, 54.7°, and 85°. It is clear from this figure that the satellite intensities are stronger at $\theta=0°$, as opposed to $\theta=85°$, indicating electron emission parallel to the electric field axis, giving rise to strongly positive β values. In our measurement, at 68.5 eV the $4s$ main line has a typical full width at half maximum (FWHM) of 142 meV, the $4p^44d(^2S_{1/2})$ FWHM is about 92-meV photon energy and the on $4p^4nd(^2S_{1/2})$ $(n=5-8)$ FWHM is on average 96 meV. The $4d$ satellite linewidth overlapped with several other lines which we did not resolve but which we took into account in our fit. They are the $4s^24p^4(^3P)5d\ ^4D_{1/2-7/2}$, the $4s^24p^4(^3P)6s\ ^2P_{1/2,3/2}$ and the $4s^24p^4(^3P)5d\ ^4F_{7/2,9/2}$. The assignments of the nd satellites are taken from Minnhagen, Strihed, and Paterson [35] and the corresponding energies from Krause *et al.* [7]. The calculated spectrum is also shown at $\theta=54.7°$. The theoretical spectrum is convoluted with a Lorentzian line shape having an arbitrary FWHM=30 meV (note that the true natural width of these lines is much less than 30 meV). This figure illustrates the good agreement between theory and experiment, and clearly shows that in many cases each experimental observed satellite consists of several excited states. The identification of the satellites is in accordance with Ref. [7], and the square of the maximal coefficient $\langle K\alpha\overline{LSJ}|\overline{EJ}\rangle$ in percents is documented in Table I. In this table all the excited states with the calculated-energy values of $E((^1D)nd\ ^2S_{1/2})\pm0.05$ eV are listed.

The absolute cross sections of the nd $(^2S_{1/2})$ $(n=4-7)$ satellites including their angular distributions are displayed in Figs. 3–6, respectively. Numerical data from our analysis are summarized in Table II. Measured intensities between the nd $(^2S_{1/2})$ satellites and the $4s$ and $4p$ main lines were converted to an absolute scale shown in the table by generating and using Bezier curves described below. Our reported $4s$ and $4p$ main line data were mostly intended to calibrate our nd satellite data. However, since other sets of data are available in the literature, we are reporting and using all of them as well as comparing them with available calculations. In our case, the $4s$ and $4p$ main line data for the cross section and the β parameter were obtained as follow, we took a complete photoelectron spectrum at 50 eV with 2-V acceleration, so that all possible electrons can be recorded. We compared the Kr $4p$ main line intensity (partial cross section) to the total intensity of the spectrum (total cross section) taking into account those electrons from above the double-ionization threshold (only half of them is included due to double photoionization). Having done so, we obtained the ratio of the $4p$ main line over the total cross section. The total cross section of krypton at 50 eV is 1.34 Mb [40], while the Kr $4p$ cross section is 74.5% of the total cross section, which gives a value of 1.0 Mb for the Kr $4p$ cross section at 50 eV. Then we took a spectra of a He-Kr mixture, and the data are included in Figs. 7–10. We then multiplied the ratio of Kr $4p$ over He $1s$ with the He $1s$ cross section, and obtained the relative cross section of the Kr $4p$ line. The β parameters were easier to obtain, since we only had to compare the Kr $4p$ and Kr $4s$ line with the He $1s$ line, and extract it from our fit as explained previously (all spectra were corrected for transmission as explained previously).

In the case of the $4s$ main line, the Bezier curve was generated from known values (Samson and Gardener [41], Tulkki *et al.* [17], Ehresmann *et al.* [42]) as well as our measured data. Figure 7 shows the Bezier curve which is represented by the dotted line. It also shows the data used (in this case Aksela *et al.*'s data [43] were not used since these data were their earlier measurements which disagreed partly with the other data sets). The figure also shows our CIPF calculation (dashed curve), where a relativistic PF approximation was used in the Kr core and in the excited atomic orbitals;

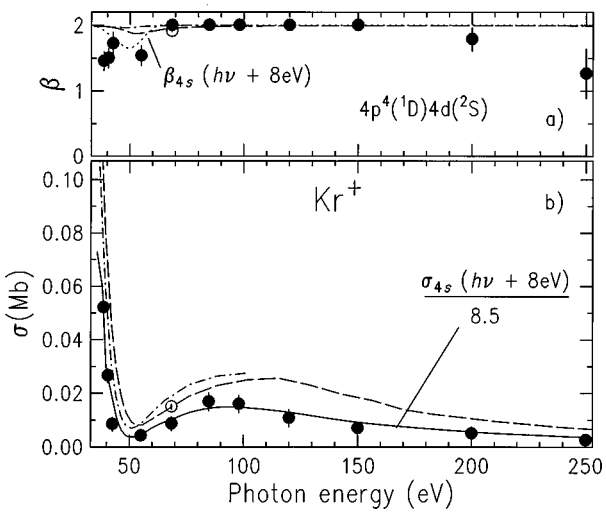

FIG. 3. (a) Angular distribution parameter β of the $4p^4(^1D)4d(^2S)$ Rydberg satellite line. The filled circles are our present measurements. The open circles was measured by Krause *et al.* [7]. The dashed curve shows the CIPF calculation. The dashed dotted curve shows the CIHF calculation. The dotted curve represents the $4s$ β parameter shifted by 8 eV. (b) Partial cross section σ of the $4p^4(^1D)4d(^2S)$ Rydberg satellite line. The filled circles are our present measurements. The open circle was measured by Krause *et al.* [7]. The dashed curve shows the CIPF calculation. The dashed dotted curve shows the CIHF calculation. The solid curve represents the $4s$ cross section scaled to 8.5 eV, and shifted by 8 eV.

TABLE I. Comparison of experimental and theoretical values for the satellites' binding energies.

State	Binding energy (eV)	
	Theory	Experiment[a]
51% $(^1D)4d(^2S_{1/2})$	33.91	33.96(3)
81% $(^1S)4d(^2D_{5/2})$	34.01	
54% $(^3P)6d(^4P_{5/2})$	36.50	
70% $(^3P)6d(^4F_{3/2})$	36.52	
63% $(^3P)6d(^4F_{5/2})$	36.52	
42% $(^1D)5d(^2S_{1/2})$	36.53	36.47(3)
59% $(^3P)7p(^4D_{5/2})$	36.55	
62% $(^3P)7p(^4P_{1/2})$	36.55	
22% $(^3P)6d(^2P_{3/2})$	36.56	
[b]12% $(^1D)5d(^2P_{1/2})$	36.57	
31% $(^3P)7p(^4S_{3/2})$	36.58	
60% $(^1D)6d(^2P_{1/2})$	37.99	
25% $(^3P)8d(^2D_{5/2})$	38.01	
68% $(^1D)6d(^2S_{1/2})$	38.03	37.82(3)
23% $(^3P)8d(^2P_{3/2})$	38.05	
83% $(^1D)7d(^2P_{1/2})$	38.73	
85% $(^1D)7d(^2D_{3/2})$	38.74	
79% $(^1D)7d(^2S_{1/2})$	38.78	38.58(3)
93% $(^1D)8d(^2D_{3/2})$	39.18	
82% $(^1D)8d(^2S_{1/2})$	39.23	39.04(3)

[a]The measured satellite energies and the designation of the satellites are taken from Ref. [7].

[b]Designation of this state is in a large extent conventional due to a small percentage of the pure basis set.

our CIHF calculation (dashed dotted curve), where a nonrelativistic Hartree-Fock approximation was used in the Kr core; and a multiconfiguration Dirac-Fock (MCDF) calculation (solid curve) by Tulkki *et al.* [17]. It is clear from this figure that the best model to the data is the CIPF calculation. In the case of the $4p$, a Bezier curve (dotted line) was generated using Samson's data [41] and our data as shown in Fig. 8 (as explained above, Aksela's data [43] were not used to generate the Bezier curve, but are displayed for comparison only). A similar procedure was done in the case of the angular distribution parameters since we needed a reference β to fit our nd satellite data. In the case of the $4s$ line, Fig. 9 shows the low-photon-energy data we used (Derenbach and Schmit [21] and our data) as well as the resulting Bezier curve (dotted curve). It also shows our CI calculation (upper dashed curve for CIHF and lower dashed for CIPF), a relativistic random-phase-approximation (RRPA) calculation by Johnson and Cheng [16] (dashed dotted curve) and Tulkki *et al.* [17] MCDF calculation (solid curve). It is clear from the figure that the models that tend to agree with the data are our CIPF and Tulkki *et al.* [17] calculations. Figure 10 shows the $4p$ angular distribution data (Miller *et al.* [44] and our data) used to generate the Bezier curve (dotted curve). It also shows a RRPA calculation (dashed curve) from Ref. [16], and a MCDF calculation (solid curve) from Ref. [17]. It is clear from the figure that the best model to the data is Tulkki *et al.*'s model. Figures 7 and 9 illustrate the influence

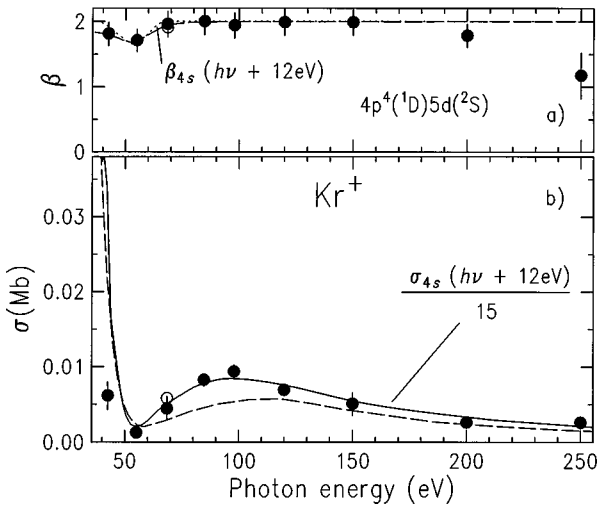

FIG. 4. (a) Angular distribution parameter β of the $4p^4(^1D)5d(^2S)$ Redberg satellite line. The filled circles are our present measurements. The open circle was measured by Krause *et al.* [7]. The dashed curve shows the CIPF calculation. The dotted curve represents the $4s$ β parameter shifted by 12 eV. (b) Partial cross section σ of the $4p^4(^1D)5d(^2S)$ Rydberg satellite line. The filled circles are our present measurements. The open circle was measured by Krause *et al.* [7]. The dashed curve shows the CIPF calculation. The solid curve represents the $4s$ cross section scaled by 15 eV and shifted by 12 eV.

of the relativistic compression of the core AO's on the values of σ and β for the main line. One can recognize that this effect leads to the decrease of the cross section after the Cooper minimum, giving a better agreement between theory and experiment. The decrease of the cross sections also leads

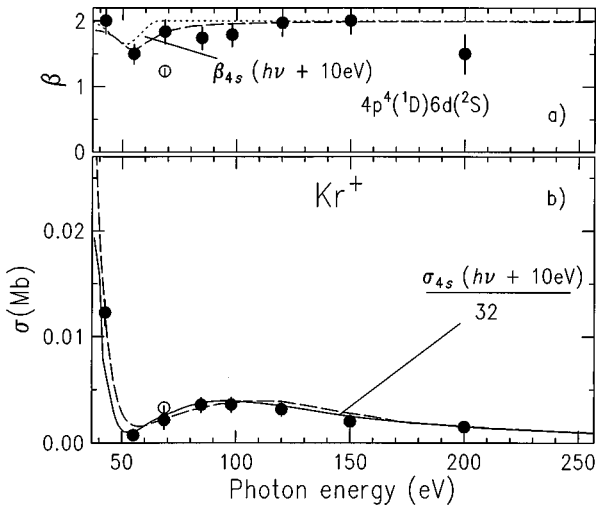

FIG. 5. Angular distribution parameter β of the $4p^4(^1D)6d(^2S)$ Rydberg satellite line. The filled circles are our present measurements. The open circle was measured by Krause *et al.* [7]. The dashed curve shows the CIPF calculation. The dotted curve represents the $4s$ β parameter shifted by 10 eV. (b) Partial cross section σ of the $4p^4(^1D)6d(^2S)$ Rydberg satellite line. The filled circles are our present measurements. The open circle was measured by Krause *et al.* [7]. The dashed curve shows the CIPF calculation. The solid curve represents the $4s$ cross section scaled by 32 eV and shifted by 10 eV.

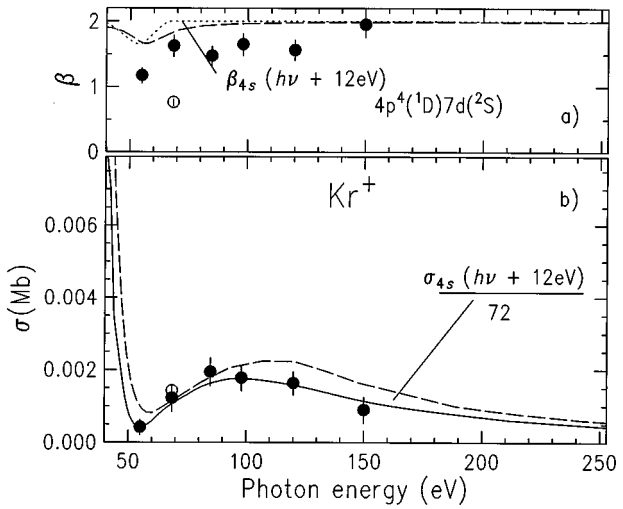

FIG. 6. Angular distribution parameter β of the $4p^4(^1D)7d(^2S)$ Rydberg satellite line. The filled circles are our present measurements. The open circle was measured by Krause *et al.* [7]. The dashed curve shows the CIPF calculation. The solid curve represents the $4s$ β parameter shifted by 10 eV. (b) Partial cross section σ of the $4p^4(^1D)7d(^2S)$ Rydberg satellite line. The filled circles are our present measurements. The open circle was measured by Krause *et al.* [7]. The dashed curve shows the CIPF calculation. The solid curve represents the $4s$ cross section scaled to 72 eV and shifted by 12 eV.

to a significant improvement in the β behavior, because the formula describing the minimum in the $\beta(\omega)$ dependence contains $\sigma(\omega)$ in the denominator [18]. The differences between the σ and β values calculated in the present paper and in Refs. [16,17] are probably connected with the fact that in those papers the DPES was not taken into account. In the case of the $4d$ satellite, Fig. 3 shows that, contrarily to the main line, relativistic compression of AO's does not play a very significant role (the CIHF and CIPF approximations are close to one another). This is connected with the fact that the nature of the dip in the $\beta(\omega)$ behavior in the case of the main line is connected mainly with the difference in the $2p_{1/2}$ and $2p_{3/2}$ AO's, whereas in the case of the $4d$ satellite, an additional large effect is connected with the significant admixture of the $2p_{1/2}$ states in the eigenvector of the $(^1D)4d\ ^2S_{1/2}$ genealogy. The admixture of the $2p_{1/2}$ states is increased in the higher $(^1D)nd\ ^2S_{1/2}$ states. Therefore, the influence of the relativistic compression of AO's on the $\beta(\omega)$ behavior for these satellites is less significant.

Figures 3–6 depict the absolute cross sections of the $nd(^2S_{1/2})$ $(n=4-7)$ satellites including their angular distributions respectively as a function of the incident photon energy. In the case of Kr, as mentioned in Sec. I, only one previous measurement at 68.5 eV is available, and is shown by the open circle in all the figures. The agreement with this measurement is very good in the case of the $5d$ satellite for both the partial cross section and the angular distribution. It is also good in the case of the $4d$ satellite. However, in the case of the $6d$ and $7d$ satellites, the agreement is good for the cross section but poor in the case of the angular distribution. This is most likely due to the lower resolution of the 90° spectrum in Ref. [7], where it becomes very difficult to disentangle the pertinent satellites from neighboring lines even with a fitting procedure. In all of the figures (Figs. 3–6) the dotted curves in part (a) represent the scaled and shifted $4s$ β parameters. The solid curves in part (b) of all the figures represent the shifted and scaled $4s$ cross section. Clearly, in all cases, we find that the absolute cross sections of these satellites lines follow very closely the shifted and scaled cross section of the $4s$ main line. However, in the case of β, we find that the nd $(^2S_{1/2})$ $(n=4,5,$ and $6)$ follow closely the β value of the $4s$ main line below 150 eV, and that only β of the $7d$ $(^2S_{1/2})$ does not. We find that the β of the nd $(^2S_{1/2})$ $(n=4,5,$ and $6)$ satellites reach $\beta=2$ below 150 eV, but this value drops significantly between 200- and 250-eV photon energy.

In all of these figures, the dashed curves represent our CIPF calculation described above. In Fig. 3, we added the CIHF calculation, which is represented by the dashed dotted curve, where the wave functions of the electrons in the continuum final states have been calculated taking into account the spin-orbit interaction of the εp electrons. While the comparison of our measurements with our calculation is good overall for all the nd satellites, some experimental trends are not reproduced by the calculation. In the case of β, the calculation agrees with the scaled curve but not with the data above 200 eV. It is interesting to note that the calculation fails to reproduce entirely the dip around 50 eV for $n=4$, but is very good for $n=5$ and 6. In the case of the cross section, the agreement is fair overall, and varies between good for the $6d$ satellite line to fair for the $4d$, $5d$, and $7d$ lines.

We interpret the discrepancies between the measurements and the calculations as follows. First, as mentioned above, the measured spectral lines consist of several lines. Therefore we need to either increase the resolution power to see the $(^1D)nd\ ^2S_{1/2}$ satellites as separate lines, or estimate σ- and β- values via the following formulas:

$$\sigma(\mathrm{Sat},\omega)=\sum_{\overline{EJ}\in \mathrm{Sat}}\sigma(\overline{EJ},\omega), \tag{4}$$

$$\beta(\mathrm{Sat},\omega)=\frac{\Sigma_{\overline{EJ}\in \mathrm{Sat}}\beta(\overline{EJ},\omega)\sigma(\overline{EJ},\omega)}{\Sigma_{\overline{EJ}\in \mathrm{Sat}}\sigma(\overline{EJ},\omega)}, \tag{5}$$

where the summation is over the states listed in Table I. Preliminary estimate showed that taking into account the overlap of the $(^1D)7d\ ^2S_{1/2}$ and $(^1D)4d\ ^2P_{1/2}$ lines only increase the dip for the $(^1D)4d\ ^2S_{1/2}$ satellite by a factor of 3, leading to a better agreement between the theory and the experiment. Second, the influence of the doubly excited states on the angular distribution parameter has to be analyzed in the range of small exciting photon energies. Third, at high photon energies one needs to analyze the intershell correlations involving the $3p$ shell, which has an ionization potential of about 200 eV, and could be significant at this energy range.

V. CONCLUSION

We have reported the measured and calculated energy dependence of the $4p^4nd(^2S_{1/2})$ $(n=4-7)$ correlation satellites in Kr from 38.5 to 250 eV. Numerical data from our analysis from 38.5 to 250 eV are summarized in Table II. Our satellite intensities are reported with respect to the $4s$

TABLE II. Comparison of experimental relative intensities, cross section, and β parameters with theoretical cross section, and β parameters for Kr $4p^4nd(^2S_{1/2})$ $(n=4-7)$ from 38.5 to 250 eV. The relative intensities are given with respect to both $4s$ and $4p$ main lines in Kr. The assignments were taken from Ref. [35], and the corresponding binding energies were taken from Ref. [7]. The uncertainty of the last digit is given in the parentheses.

		Relative intensity			σ (kB)		β		
			$I(4S)=100$					Experiment	
Photon energy (eV)	Assignment[a] $(^1D)nd(^2S_{1/2})$	$I(4p)=100$ This work	This work	Ref. [7]	Theory This work	Experiment This work	Theory This work	This work	Ref. [7]
	$n=4$	1.11(10)	87(9)		98.56	52(3)	1.979	1.45(14)	
38.5	$n=5$				43.67		1.822		
	$n=6$				27.28		1.854		
	$n=7$				21.39		1.906		
	$n=4$	0.68(10)	80(8)		66.19	27(3)	1.973	1.50(15)	
40.5	$n=5$				30.75		1.807		
	$n=6$				18.27		1.844		
	$n=7$				14.83		1.902		
	$n=4$	0.34(10)	25(3)		42.68	8.5(25)	1.964	1.72(17)	
42.5	$n=5$	0.25(10)	17.6(17)		20.46	6.1(18)	1.789	1.80(18)	
	$n=6$	0.51(10)	33(3)		12.58	12.2(12)	1.822	2.0(2)	
	$n=7$				10.25		1.889		
	$n=4$	0.66(10)	6.6(7)		8.17	4.2(12)	1.879	1.54(15)	
55.0	$n=5$	0.19(10)	1.9(2)		2.38	1.2(4)	1.694	1.70(17)	
	$n=6$	0.11(10)	1.1(1)		1.65	0.7(3)	1.569	1.49(14)	
	$n=7$	0.06(1)	0.6(1)		1.00	0.4(1)	1.674	1.17(11)	
	$n=4$	2.7(2)	8.4(8)	13.7(7)	14.84	8.7(26)	1.951	2.0(2)	1.91(1)[b]
68.5	$n=5$	1.4(2)	4.5(4)	5.3(3)	2.92	4.4(13)	1.946	1.95(19)	1.90(4)
	$n=6$	0.68(10)	2.2(2)	3.0(2)	2.26	2.1(6)	1.832	1.83(18)	1.23(5)
	$n=7$	0.39(10)	1.2(1)	1.3(1)	1.15	1.2(3)	1.837	1.62(16)	0.76(6)
	$n=4$	6.1(6)	14.8(15)		21.69	17(3)	1.978	2.0(2)	
84.8	$n=5$	2.9(3)	7.3(7)		4.55	8.2(8)	1.989	1.99(19)	
	$n=6$	1.3(1)	3.1(3)		3.28	3.5(7)	1.932	1.73(17)	
	$n=7$	0.7(10)	1.7(2)		1.79	1.9(3)	1.939	1.47(14)	
	$n=4$	15.2(15)	12.9(13)		24.4	16(3)	1.985	2.0(2)	
98	$n=5$	2.9(3)	7.8(8)		5.34	9.3(9)	1.994	1.93(19)	
	$n=6$	1.1(1)	3.2(3)		3.77	3.6(7)	1.957	1.78(17)	
	$n=7$	0.5(5)	1.5(1)		2.12	1.8(4)	1.962	1.64(16)	
	$n=4$	3(3)	9.5(9)		24.78	11(3)	1.991	2.0(2)	
120	$n=5$	1.9(2)	6.1(6)		5.66	6.9(7)	1.995	1.98(19)	
	$n=6$	0.87(10)	2.7(3)		3.90	3.1(6)	1.976	1.96(19)	
	$n=7$	0.49(10)	1.3(1)		2.23	1.6(3)	1.962	1.55(15)	
	$n=4$	3.2(3)	7.7(8)		18.45	7(2)	1.994	2.0(2)	
150	$n=5$	2.3(2)	5.5(5)		4.24	5(2)	1.995	1.98(19)	
	$n=6$	0.9(1)	2.2(2)		2.79	1.9(8)	1.986	2.0(2)	
	$n=7$	0.4(1)	0.97(10)		1.64	0.9(4)	1.987	1.94(19)	
	$n=4$	4.2(4)	11.3(11)		10.58	5(2)	1.994	1.79(17)	
200	$n=5$	3.3(3)	5.9(6)		2.38	2.6(8)	1.995	1.78(17)	
	$n=6$	0.9(2)	2.2(4)		1.57	1.5(6)	1.991	1.50(29)	
	$n=7$				0.902		1.991		
	$n=4$	4.6(14)	14(4)		6.78	2.5(8)	1.994	1.27(38)	
250	$n=5$	3.2(10)	9(3)(4)		1.53	2.6(8)	1.995	1.17(35)	
	$n=6$				1.01		1.991		
	$n=7$				0.578		1.991		

[a]Minnhagen, Strihed, and Petersson [35].

[b]Average β of two combined states.

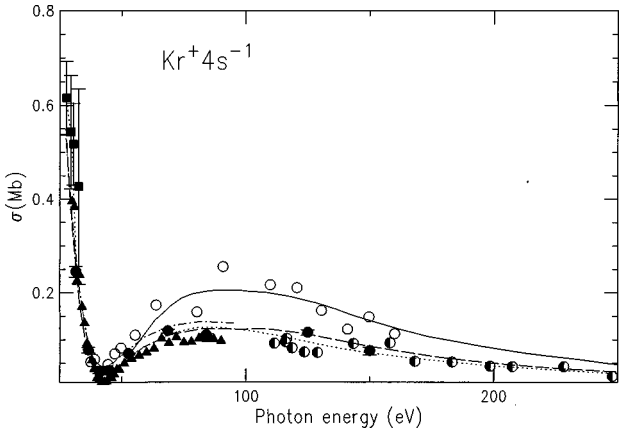

FIG. 7. The ionization cross section of the $4s$ electron as a function of exciting photon energy. The open circles were measured by Aksela *et al.* [43]. The filled squares were measured by Samson [40]. The half-filled circles were measured by Tulkki *et al.* [17]. The filled triangles are measured by Ehresmann *et al.* [42]. The filled circles are our present measurements. The dashed curve shows the CIPF calculation. The dashed dotted curve shows the CIHF calculation. The solid curve shows the MCDF calculation of Tulkki *et al.* [17]. The dotted curve is the Bezier curve adapted to the average of all the experimental data except Ref. [43] (see text for detail).

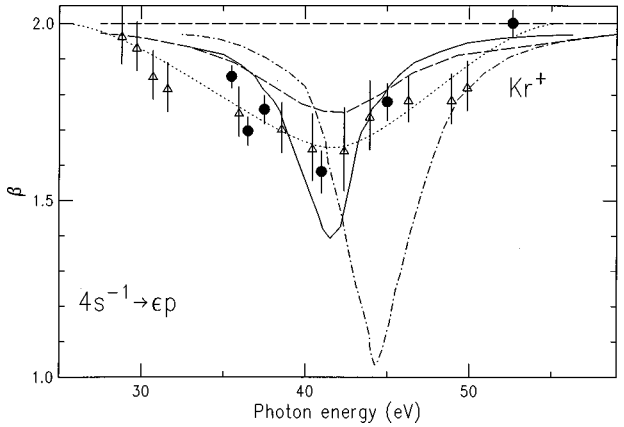

FIG. 9. Angular distribution parameter β for the $4s$ main line as a function of exciting photon energy. The open triangles were measured by Derenbach and Schmit [21]. The filled circles are our present measurements. The upper dashed curve shows the CIHF calculation. The lower dashed curve shows the CIPF calculation. The dashed dotted curve shows the RRPA calculation of Johnson and Cheng [16]. The solid curve shows the MCDF calculation of Tulkki *et al.* [17]. The dotted curve is the Bezier curve adapted to the average of all experimental data (see text for detail).

and $4p$ main lines, and are compared with the results of Krause *et al.* [7] at 68.5 eV. As mentioned above the agreement with Ref. [7] is good to poor, probably due to a contribution of overlapping lines. In our analysis we made an effort to single out the $4d$ line from the other nearby lines overlapping with the $4d$ satellite. These lines are the $4s^2 4p^4(^3P)5d\ ^4D_{1/2-7/2}$, the $4s^2 4p^4(^3P)6s\ ^2P_{1/2,3/2}$ and the $4s^2 4p^4(^3P)5d\ ^4F_{7/2,9/2}$. From the table we can see that the calculation for some satellites at energies below 68.5 eV are overestimated. However, at and above 68.5 eV the agreement is fairly good. This is similar to the CI calculations of Smid and Hansen [26], but is not as extensive. We also list measured and calculated absolute cross sections (calibrated as described above) and calculated and measured β values. The agreement varies as described in the text. The behavior of these satellites lines follows closely the $4s$ main line. The agreement between the CI calculation and the measurements is good overall. We hope that an improvement in the experimental resolution in the future will resolve overlapping components, leading to a better determination of the β parameters to allow for a better comparison between theory and experiment. From the theoretical point of view the calculation involving $3p$ shell in the intershell correlations could be also interesting.

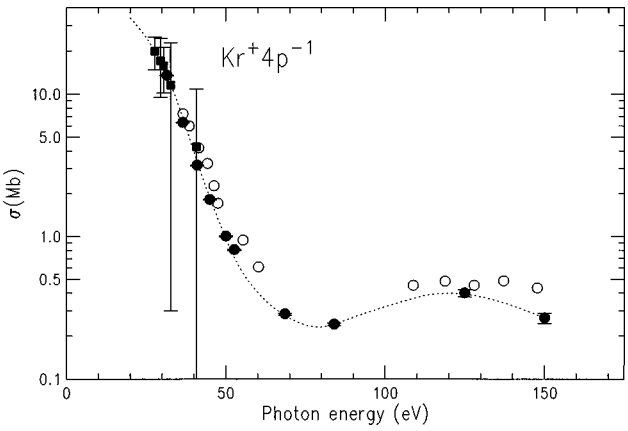

FIG. 8. The ionization cross section of the $4p$ electron as a function of exciting photon energy. The open circles were measured by Aksela *et al.* [43]. The filled squares were measured by Samson [41]. The filled circles are our present measurements. The dotted curve is the Bezier curve which was adapted to the data of Samson [41] in the low-energy range ($h\nu < 40$ eV), and to our data for higher photon energies (see text for detail).

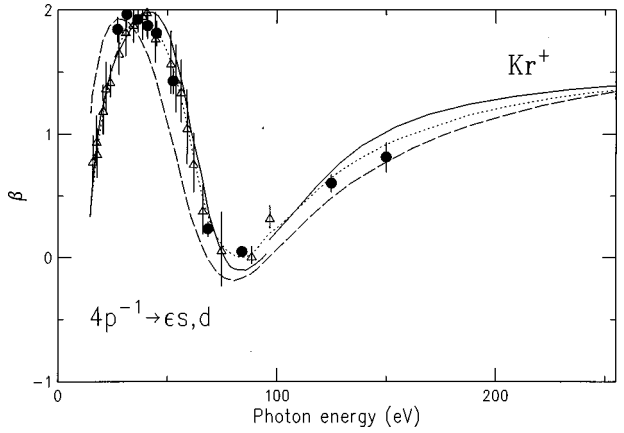

FIG. 10. Angular distribution parameter β for the $4p$ main line as a function of photon energy. The open triangles were measured by Miller *et al.* [44]. The filled circle are our present measurements. The dashed curve shows (RRPA) calculation of Johnson and Cheng [16]. The solid curve shows the MCDF calculation of Tulkki *et al.* [17]. The dotted curve is the Bezier curve adapted to the average of all experimental data (see text for detail).

ACKNOWLEDGMENTS

This work was supported by the U.S. Department of Energy, Office of Basic Energy Science, Division of Chemical Sciences, under Contract No. DE-FG02-95ER14299, by the Bundesminister für Forschung und Technologie, and by the Deutsche Forschungsgemeinschaft. N.B., B.L., and S.B.W. are grateful to the Alexander von Humboldt Foundation for support.

[1] T. A. Carlson, Phys. Rev. **156**, 142 (1967).
[2] M. O. Krause, T. A. Carlson, and R. D. Dismukes, Phys. Rev. **170**, 37 (1968).
[3] S. Svensson, B. Eriksson, N. Martensson, G. Wendin, and U. Gelius, J. Electron Spectrosc. Relat. Phenom. **47**, 327 (1988).
[4] U. Becker, B. Langer, H. G. Kerkhoff, M. Kupsch, D. Szostak, R. Wehlitz, P. A. Heimann, S. H. Liu, D. W. Lindle, T. A. Ferret, and D. A. Shirley, Phys. Rev. Lett. **60**, 1490 (1988).
[5] A. A. Wills, A. A. Cafolla, F. J. Curell, J. Comer, A. Svensson, and M. A. MacDonald, J. Phys. B **22**, 3217 (1989).
[6] R. I. Hall, L. Avaldi, G. Dawber, M. Zubek, and G. C. King, J. Phys. B **23**, 4469 (1990).
[7] M. O. Krause, S. B. Whitfield, C. D. Caldwell, J.-Z. Wu, P. Van der Meulen, C. A. de Lange, and R. W. C. Hansen, J. Electron Spectrosc. Relat. Phenom. **58**, 79 (1992).
[8] A. A. Wills, A. A. Cafolla, and J. Comer, J. Phys. B **23**, 2029 (1990).
[9] S. T. Manson, J. Electron Spectrosc. Relat. Phenom. **9**, 21 (1976).
[10] A. F. Starace, in *Corpuscels and Radition in matterI Handbuch der Physik*, edited by W. Melhom (Springer-Verlag, Berlin, 1982), Vol. XXXI, pp. 1–121.
[11] K. G. Dyall and F. P. Larkins, J. Phys. B **15**, 219 (1982).
[12] J. Tulkki, Phys. Rev. Lett. **62**, 2817 (1989).
[13] V. L. Sukhorukov, B. M. Lagutin, I. D. Petrov, H. Schmoranzer, A. Ehresmann, and K. H. Schartner, J. Phys. B **27**, 241 (1994), and references therein.
[14] T. E. H. Walker and J. T. Waber, J. Phys. B **6**, 1165 (1973).
[15] N. A. Cherepkov, Phys. Rev. Lett. **66A**, 204 (1978).
[16] W. R. Johnson and K. T. Cheng, Phys. Rev. A **20**, 978 (1979).
[17] J. Tulkki, S. Aksela, H. Aksela, E. Shigemasa, A. Yagishita, and Y. Furusawa, Phys. Rev. A **45**, 4640 (1992).
[18] B. M. Lagutin, I. D. Pertov, V. L. Sukhorukov, S. B. Whitfield, B. Langer, J. Viefhaus, R. Wehlitz, N. Berrah, W. Mahler, and U. Becker, J. Phys. B **29**, 937 (1996).
[19] J. L. Dehmer and D. Dill, Phys. Rev. Lett. **37**, 1049 (1976).
[20] H. Derenbach and V. Schmit, J. Phys. B **16**, L337 (1983).
[21] H. Derenbach and V. Schmit, J. Phys. B **17**, 83 (1984).
[22] M. Y. Adam, F. Wuilleumier, N. Sandner, V. Schmidt, and G. Wendin, J. Phys. (Paris) **39**, 129 (1978).
[23] H. Kossman, B. Krassig, V. Schmidt, and J. E. Hansen, Phys. Rev. Lett. **58**, 1620 (1987).
[24] C. E. Brion, K. H. Tan, and G. M. Bancroft, Phys. Rev. Lett. **56**, 584 (1986).
[25] B. Langer, J. Viefhaus, O. Hemmers, A. Menzel, R. Wehlitz, and U. Becker, Phys. Rev. A **51**, R882 (1995).
[26] H. Smid and J. E. Hansen, Phys. Rev. Lett. **52**, 2138 (1984).
[27] W. Wijesundera and H. P. Kelly, Phys. Rev. A **39**, 634 (1989).
[28] V. L. Sukhorukov, B. M. Lagutin, H. Schmoranzer, I. D. Petrov, and K. H. Schartner, Phys. Lett. **169**, 445 (1992).
[29] S. B. Whitfield, B. Langer, J. Viefhaus, R. Wehlitz, N. Berrah, W. Mahler, and U. Becker, J. Phys. B **27**, L359 (1994), and references therein.
[30] D. P. Spears, H. J. Fishbeck, and T. A. Carlson, Phys. Rev. A **9**, 1603 (1974).
[31] T. Möler, Synch. Radiat. News **6**, 16 (1993).
[32] U. Becker, D. Szostak, H. G. Kerkhoff, M. Kupsch, B. Langer, R. Wehlitz, A. Yagishita, and T. Hayaishi, Phys. Rev. A **39**, 3902 (1989).
[33] G. V. Marr and J. B. West, At. Data **18**, 497 (1976).
[34] F. Wuilleumier and M. O. Krause, J. Electron Spectrosc. Relat. Phenom. **15**, 15 (1979).
[35] L. Minnhagen, H. Strihed, and B. Petersson, Ark. Fys. **39**, 34 (1968).
[36] H. Schmoranzer, A. Ehresmann, F. Vollweiler, V. L. Sukhorukov, B. M. Lagutin, I. D. Petrov, K.-H. Schartner, and B. Möbus, J. Phys. B **26**, 2795 (1993).
[37] R. Kau, I. D. Petrov, V. L. Sukhorukov, and H. Hotop, Z. Phys. D **39**, 267 (1997).
[38] R. Kau, I. D. Petrov, V. L. Sukhorukov, and H. Hotop, J. Phys. B **29**, 5673 (1996).
[39] J. Sugar and A. Musgrove, J. Chem. Ref. Data **20**, 859 (1991).
[40] J. A. R. Samson (private communication).
[41] J. A. R. Samson and J. L. Gardner, Phys. Rev. Lett. **33**, 671 (1974).
[42] A. Ehresmann, F. Vollweiller, H. Schmoranzer, V. L. Sukhorukov, B. M. Lagutin, I. D. Petrov, G. Mentzel, and K.-H. Schartner, J. Phys. B **27**, 1489 (1994).
[43] S. Aksela, H. Aksela, M. Levasalmi, K. H. Tan, and G. M. Bancroft, Phys. Rev. A **36**, 3449 (1987).
[44] D. L. Miller, J. D. Dow, R. G. Houlgate, G. V. Marr, and J. B. West, J. Phys. B **10**, 3205 (1977).